



## OPEN ACCESS

## EDITED BY

Marcelo Ezquer,  
University for Development, Chile

## REVIEWED BY

Yana Olegovna Mukhamedshina,  
Kazan Federal University, Russia  
Wu Zhou,  
The First Affiliated Hospital of Nanchang  
University, China

## \*CORRESPONDENCE

Bo Fang

✉ bfang@cmu.edu.cn

<sup>†</sup>These authors have share first authorship

RECEIVED 19 January 2025

ACCEPTED 04 April 2025

PUBLISHED 13 May 2025

## CITATION

Hao X, Cao L, Li J, Lei Q, Liu X, Li Y, Fan Y,  
Xu J and Fang B (2025) FOXA2/miR-148a-3p/  
SMURF2 signaling feed-forward loop  
alleviates spinal cord ischemia-reperfusion  
injury-induced neuropathic pain by  
modulating microglia polarization in rats.  
*Front. Immunol.* 16:1563377.  
doi: 10.3389/fimmu.2025.1563377

## COPYRIGHT

© 2025 Hao, Cao, Li, Lei, Liu, Li, Fan, Xu and  
Fang. This is an open-access article distributed  
under the terms of the [Creative Commons  
Attribution License \(CC BY\)](#). The use,  
distribution or reproduction in other forums  
is permitted, provided the original author(s)  
and the copyright owner(s) are credited and  
that the original publication in this journal is  
cited, in accordance with accepted academic  
practice. No use, distribution or reproduction  
is permitted which does not comply with  
these terms.

# FOXA2/miR-148a-3p/SMURF2 signaling feed-forward loop alleviates spinal cord ischemia- reperfusion injury-induced neuropathic pain by modulating microglia polarization in rats

Xiaotong Hao<sup>†</sup>, Linyan Cao<sup>†</sup>, Jinshi Li, Qian Lei, Xuan Liu,  
Yuanyuan Li, Yiting Fan, Jingjing Xu and Bo Fang\*

Department of Anesthesiology, The First Hospital of China Medical University, Shenyang,  
Liaoning, China

**Background:** Microglia polarization is crucial in mediating neuropathic pain. However, the role of microglia polarization in regulating spinal cord ischemia-reperfusion injury (SCIRI)-induced neuropathic pain is largely unknown. This study aimed to elucidate the relationship between SCIRI-induced neuropathic pain and microglia polarization, as well as the underlying mechanisms, with the objective of identifying potential therapeutic targets.

**Methods:** A rat model of SCIRI was established by aortic arch clamping, then pain thresholds were measured. *In vitro*, oxygen-glucose deprivation/reperfusion (OGD/R) of HAPI microglia was performed. The expressions of sirtuin1 (SIRT1), SMAD specific E3 ubiquitin protein ligase 2 (SMURF2), and markers of microglial polarization (CD206, iNOS) were quantitated by Western blot and immunofluorescence, and the levels of cytokines (TNF- $\alpha$ , IL-4) were assessed by Enzyme-linked immunosorbent assay (ELISA). Real-time quantitative reverse transcription PCR (RT-qPCR) experiments were conducted to quantify the levels of miR-148a-3p and FOXA2. Dual-luciferase reporter assay was employed to identify the targeted regulation of SMURF2 by miR-148a-3p and the transcriptional regulation of miR-148a-3p by FOXA2. The regulatory role of FOXA2 in the transcription of miR-148a-3p was validated using chromatin immunoprecipitation (ChIP). In addition, co-immunoprecipitation (Co-IP) assays were performed to confirm the binding relationship between SMURF2 and FOXA2. And the ubiquitination levels of FOXA2 and SIRT1 were measured. Subsequently, rats were administered miR-148a-3p to assess pain thresholds. Western blot and immunofluorescence quantitative analysis was conducted to assess the expression of markers associated with microglia polarization.

**Results:** SCIRI significantly reduced mechanical and thermal pain thresholds in rats and promoted microglial polarization, with a concomitant decrease in SIRT1 expression and an increase in SMURF2 expression in microglial cells. Further analysis revealed that upregulation of miR-148a-3p promoted microglia polarization toward M2 by targeting SMURF2, which in turn inhibited ubiquitination of SIRT1. FOXA2 was an upstream transcription factor of miR-

148a-3p and SMURF2 bound to FOXA2, resulting in its ubiquitination. Finally, *in vivo* experiments demonstrated that miR-148a-3p effectively promoted microglia transformation from M1 to M2 and reduced neuropathic pain following SCIRI.

**Conclusions:** The FOXA2/miR-148a-3p/SMURF2 signaling feed-forward loop regulates SIRT1 levels and thereby exerts control over microglia polarization and the regulation of SCIRI-induced neuropathic pain.

#### KEYWORDS

**smurf2, SIRT1, miR-148a-3p, foxa2, spinal cord ischemia-reperfusion injury, neuropathic pain, microglia polarization**

## 1 Introduction

Spinal cord ischemia-reperfusion injury (SCIRI) represents a significant adverse consequence of thoracoabdominal aortic surgery and spinal cord decompression surgery (1). Previous studies have concentrated on SCIRI-induced motor pathologies, such as paraplegia and paralysis (2). Nevertheless, it is imperative to recognize that neuropathic pain is also a prominent symptom of SCIRI, which can significantly impair the quality of life of patients (3, 4). Neuropathic pain, is a pathological condition triggered by injuries or diseases impacting the somatosensory system, presents symptoms including allodynia and hyperalgesia (5, 6). Recent research has emphasized the critical role of microglia in the progression of neuropathic pain. For instance, microglia, which lead to the degradation of the network around neurons, and microglia chemokines, all influence the occurrence of neuropathic pain (7, 8). As resident immune sentinels in the central nervous system (9), microglia exhibit remarkable phenotypic plasticity. Timothy R. et al. identified a microglial subpopulation that exhibited distinctive inflammatory signaling characteristics, as determined by single-cell sequencing techniques. This subpopulation may play a specific role in initiating inflammatory responses (10). Under pathological conditions, microglia undergo polarization into two classical phenotypes: the pro-inflammatory M1-type (characterized by inducible nitric oxide synthase (iNOS) expression) that exacerbates neural damage through tumor necrosis factor- $\alpha$  (TNF- $\alpha$ ) release (11–13), and the anti-inflammatory M2-type (marked by CD206) that promotes neural repair via protective mediators like interleukin-4 (IL-4) (14–16). It is important to acknowledge that, subsequent to SCIRI, in addition to the classical M1/M2 phenotype (17), there are also intermediate M1/2 microglia with dual phenotypic characteristics (18). A number of signaling factors and compounds have been demonstrated to modulate neuropathic pain by modulating M1/M2 polarization. These include TRAF6 (19), Huangqin declination (20), and DUSP1 (21), botulinum toxin (22), among others. These studies suggest

that this dynamic phenotypic shift in M1/M2 may constitute an important regulatory node for the development of neuropathic pain (23).

Mammalian cell sirtuin1 (SIRT1) is a kind of deacetylase dependent on nicotinamide adenosine dinucleotide (NAD<sup>+</sup>). SIRT1 has been known to be involved in neuroinflammation, which can inhibit microglia activation and other inflammatory reactions (24–26), and relieve neuropathic pain through a variety of signal pathways, such as the NF- $\kappa$ B, p53 and PI3K/AKT (4, 27, 28). In addition, overexpression of SIRT1 promotes microglia to M2 type polarization (29). SMAD ubiquitin regulatory factor 2 (SMURF2) has been shown to function as an E3 ubiquitin ligase, associated with post-ischemic neural damage (30, 31) and inflammation (32, 33), and regulates protein expression in macrophages (34). Recent evidence reported that SMURF2 has a specific binding affinity for SIRT1 and induces its ubiquitin-mediated degradation (35). However, the potential involvement of SIRT1 is poorly elucidated in neuropathic pain.

Specific miRNAs have been the subject of considerable interest due to their capacity to influence pain perception. For example, the miRNA-22/MTF1 signaling axis has been identified as a key player in the initiation and maintenance of inflammatory pain in the spinal dorsal horn (36). Conversely, miR-32-5p downregulation in trigeminal ganglion neurons has been shown to regulate trigeminal neuropathic pain (37). These findings highlight the complex and multifaceted roles of miRNAs in pain modulation. FOXA is a member of the forkhead box protein family, which includes FOXA1, FOXA2, and FOXA3. It has a wide range of functions, including roles in development, glycolipid metabolism, the aging process, and immune regulation. Despite the existence of numerous reports investigating the interaction between FOXA and miRNAs (38, 39), the functional role of these interactions in neuropathic pain, particularly in SCIRI, has yet to be elucidated.

The aim of this study was to explore the molecular mechanism of neuropathic pain after SCIRI, so as to explore promising therapeutic targets for neuropathic pain.

## 2 Materials and methods

### 2.1 Experimental animals and ethics statement

In this study, Sprague-Dawley (SD) rats weighing between 200–250 g were utilized as the primary experimental animals. These rats were procured from the Experimental Animal Center of the China Medical University (Shenyang, China). The animals were housed in standard cages under controlled environmental conditions: a temperature of  $22 \pm 2^\circ\text{C}$ , humidity levels maintained at  $50 \pm 10\%$ , and a 12 h/12 h light/dark cycle. Before initiating the experiments, the rats were given a week-long acclimatization period where they were allowed ad libitum access to both food and water. All surgical interventions were conducted under anesthesia to minimize pain and distress to the animals. The experimental protocols, especially those involving animal handling and procedures, were approved by the Animal Care and Use Committee of China Medical University.

### 2.2 Rat model of SCIRI

The aortic cross-clamping method was utilized to induce SCIRI (40). Rats were anesthetized through intraperitoneal injection of 4% pentobarbital sodium at a dose of 50 mg/kg. The rectal temperature was diligently maintained at  $37 \pm 0.5^\circ\text{C}$  throughout the surgical procedure using a heating lamp. Once anesthetized, rats were positioned in lateral recumbency, and the aortic arch was exposed via a cervicothoracic approach. Clamping was executed between the left common carotid artery and the left subclavian artery, sustained for a period of 8 minutes.

### 2.3 Intrathecal injection

A total of four days prior to the administration of SCIRI, rats were anesthetized with 3% isoflurane. An intrathecal catheter was then placed in the L5-L6 intervertebral space. Injections were administered at 12 h intervals between each, and the injections spanned three consecutive days. Each injection encompassed 10  $\mu\text{L}$  of either miR-148a-3p mimic or NC mimic, at a concentration of 50  $\mu\text{mol/L}$  with invitroRNA<sup>TM</sup> (InvivoGene Biotechnology, Nanjing, China).

### 2.4 Nociceptive behavioral testing

Prior to the commencement of the experiment, the rats were acclimatized to the environment for a period of one hour. Mechanical sensitivity was assessed using the paw withdrawal threshold (PWT), defined as the force (g) causing the rat to retract its paws. PWT was measured using von Frey filaments (Anesthesio, Danmic Global, USA), which were gently lifted upward perpendicular to the sole of the mouse until the filaments were bent. Positive responses, indicated by avoidance movements such as retraction, shaking, or licking of the affected limb, were

recorded. The measurements were repeated four times at this stimulus intensity, and the average PWT was calculated.

Thermal sensitivity was assessed 15 minutes after the PWT measurement using the paw withdrawal latency (PWL) method. PWL denotes the duration taken for a rat to conspicuously retract its paw when placed on a hot plate (YAN-6B, YUYAN Shanghai, China) set at  $50^\circ\text{C}$ . To prevent potential tissue damage, the maximum exposure time on the hot plate was capped at 25 seconds. This measurement was taken three times with a 10 minutes interval between each to compute the average PWL. All behavioral tests were administered in a blinded manner.

### 2.5 Experimental protocols

#### 2.5.1 Protocol I

Rats were randomly divided into a Sham group ( $n = 6$ ) and a SCIRI group ( $n = 6$ ). The SCIRI group underwent the SCIRI procedure, while the sham group underwent the same procedure except that the aorta was clamped. PWT and PWL were measured in the hindpaw 6 hours before SCIRI and 8 hours, 16 hours, and on days 1, 2, 3, 5, and 7 after SCIRI. Additionally, rats were euthanized at 6 hours before SCIRI and at 8 hours, 16 hours, as well as on days 1, 3, and 5 after SCIRI to obtain spinal cord tissue for Western blot analysis. Spinal cord tissue on day 3 after SCIRI was used for immunofluorescence analysis (Figures 1, 2).

#### 2.5.2 Protocol II

Rats were divided into 4 groups ( $n = 6$  rats/group): sham; SCIRI; SCIRI treated with miR-mimic (SCIRI + miR-mimic); SCIRI treated with NC mimic (SCIRI + NC mimic). PWT and PWL were assessed in the hindpaw 6 hours before SCIRI and 8 hours, 16 hours, and days 1, 2, 3, 5, and 7 after SCIRI. Rats in the SCIRI, SCIRI + miR-mimic, and SCIRI + NC mimic groups were euthanized on day 3 post-SCIRI for Western blot analysis, ELISA, and immunofluorescence (Figure 3).

### 2.6 Cell culture and transfection

HAPI, HEK293T and VSC4.1 cells were cultured in Dulbecco's Modified Eagle Medium (DMEM) obtained from Procell Company, Wuhan, China. The culture medium was supplemented with 10% Fetal Bovine Serum (FBS) and 100 U/ml of penicillin/streptomycin. Cells were maintained according to the supplier's recommendations. For transfection experiments, cells were transfected with small interfering RNA using invitroRNA<sup>TM</sup> (InvivoGene Biotechnology, Nanjing, China) following the manufacturer's guidelines.

### 2.7 Oxygen-glucose deprivation/reperfusion

HAPI cells were cultured in a serum-free and glucose-free DMEM medium and then placed into a sterile three-gas

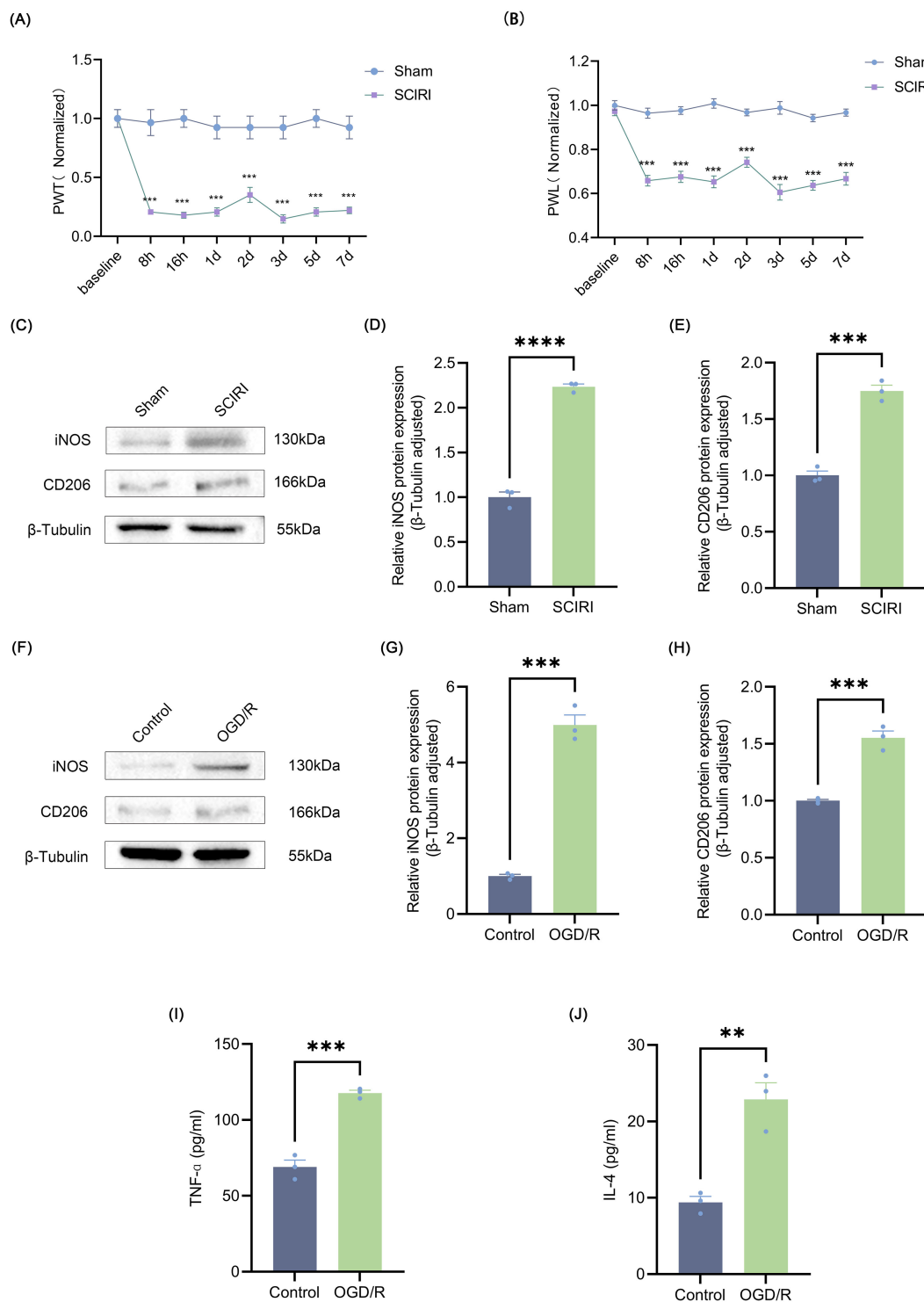


FIGURE 1

SCIRI induces neuropathic pain and microglia polarization. **(A, B)** Changes in PWT and PWL after SCIRI in rats. Data are expressed as normalized values against their respective Sham. **(C)** Representative Western blot bands representing temporal expression changes of iNOS and CD206 in the spinal cord of rats following SCIRI. **(D, E)** Quantitative protein analysis of iNOS and CD206 in the spinal cord of rats following SCIRI. **(F)** Representative Western blot of iNOS and CD206. **(G, H)** Quantitative protein analysis of iNOS and CD206 in the HAPI following OGD/R. **(I, J)** HAPI cells supernatant TNF- $\alpha$  and IL-4 are detected by ELISA. Repeated-measures analysis of variance was utilized in **(A, B)**  $n=6$  in each group. Unpaired t-test was utilized. Significance levels: \*\* $P<0.01$ , \*\*\* $P<0.001$ , \*\*\*\* $P<0.0001$ .

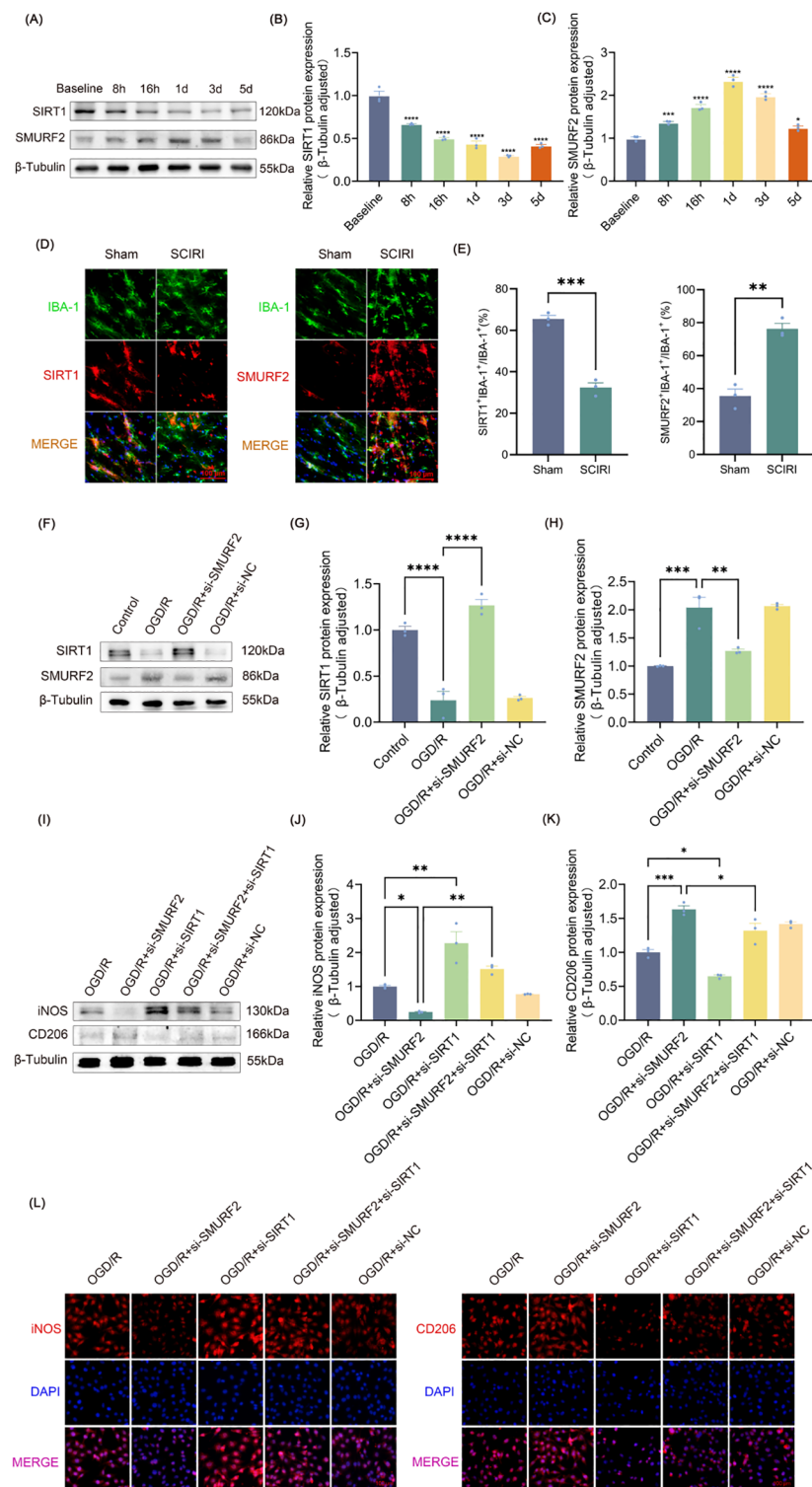


FIGURE 2

SMURF2 regulates microglia polarization by downregulating SIRT1 after SCIRI. **(A)** Representative Western blot bands representing temporal expression changes of SIRT1 and SMURF2 in the spinal cord of rats following SCIRI. **(B, C)** Quantitative protein analysis of SIRT1 and SMURF2 in the spinal cord of rats following SCIRI. **(D)** Immunofluorescence revealed the co-expression of SIRT1 or SMURF2 and IBA-1 in the rat spinal cord three days after SCIRI. Scale bar: 100  $\mu$ m. **(E)** Quantitative fluorescence area analysis. **(F)** Representative Western blot of SIRT1 and SMURF2. **(G, H)** Quantitative protein analysis of SIRT1 and SMURF2. **(I)** Representative Western blot of iNOS and CD206. **(J, K)** Quantitative protein analysis of iNOS and CD206. **(L)** Immunofluorescence revealed iNOS-positive and CD206-positive microglial cells. Scale bar: 100  $\mu$ m. Unpaired t-test and one-way ANOVA were utilized. Significance levels: \*P<0.05, \*\*P<0.01, \*\*\*P<0.001, \*\*\*\*P<0.0001.



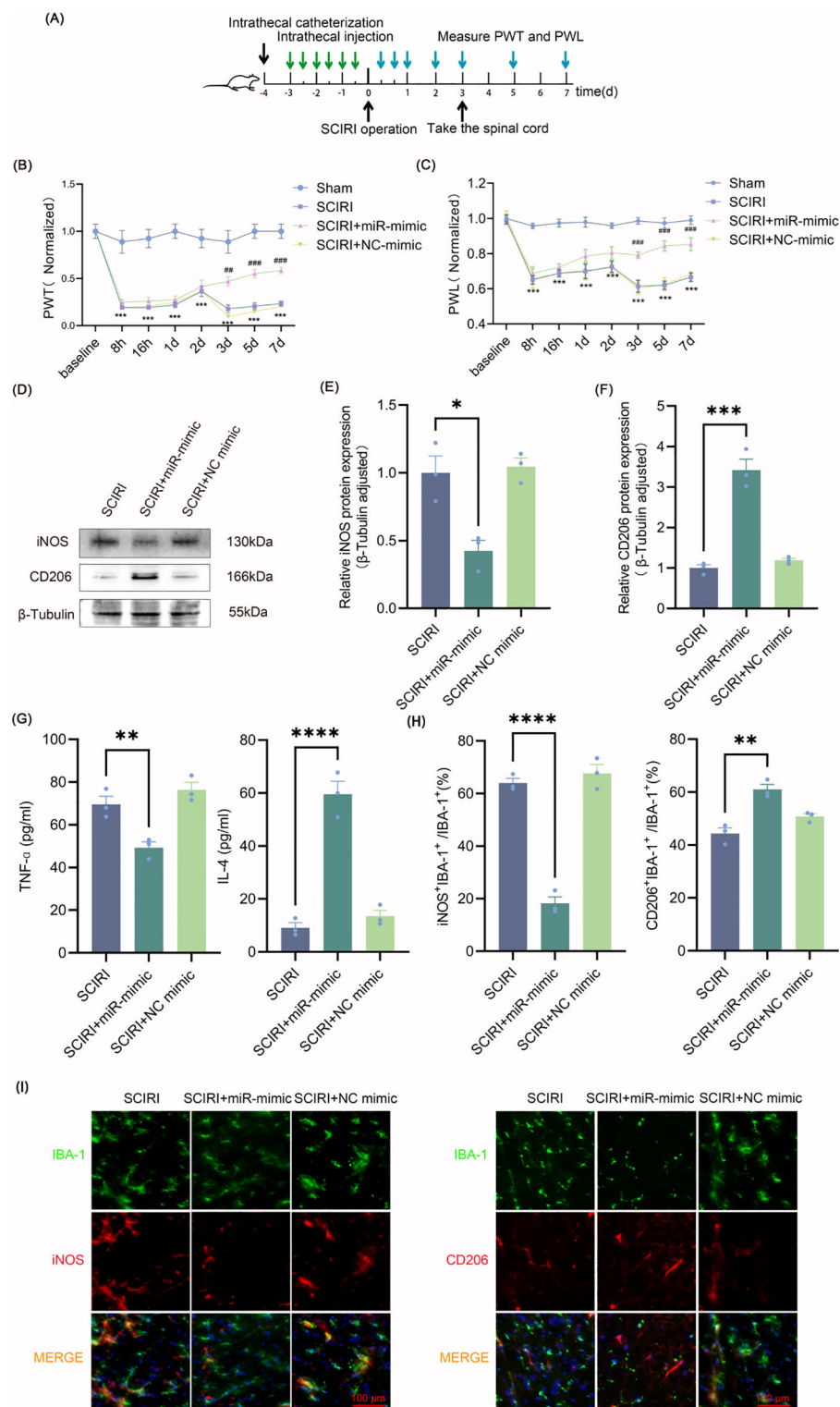


FIGURE 3

Intrathecal injection of miR-148a-3p polarizes spinal microglia to M2 and relieves neuropathic pain after SCI. **(A)** Process schematic. **(B, C)** Changes of PWT and PWL over time in rats. Data are expressed as normalized values against their respective Sham. **(D)** Representative Western blot of iNOS and CD206 in the spinal cords of rats. **(E, F)** Quantitative protein analysis of iNOS and CD206. **(G)** Evaluation of microglia polarization markers by ELISA. **(H)** Quantitative fluorescence area analysis. **(I)** Immunofluorescence co-localization revealed iNOS-positive and CD206-positive microglial cells. Scale bar: 100 μm. Repeated-measures analysis of variance was utilized in **(B, C)**  $n=6$  in each group. One-way ANOVA was used in **E-H**. Significance levels: \* $P<0.05$ , \*\* $P<0.01$ , \*\*\* $P<0.001$ , \*\*\*\* $P<0.0001$ . \*\*\* $p<0.001$  Sham versus SCI, and ### $p<0.01$ , ### $p<0.001$  SCI versus SCI+miR-mimic in **(B, C)**.

incubator (94%N<sub>2</sub>, 5%CO<sub>2</sub>, 1%O<sub>2</sub>), incubated at 37°C for 4 h to induce OGD injury. The cells were then returned to a 37°C, 5% CO<sub>2</sub> incubator and incubated in a normal medium for a 24 h reperfusion period. The control HAPI was grown in a normoxic incubator in a medium containing glucose for the same time period.

## 2.8 Western blot

The extracted spinal cord tissue from the expanded segment (L4-6) of rats and cell samples were meticulously placed in 1.5mL EP tubes. The protein plasma was collected by means of centrifugation after protein extraction using Radioimmunoassay (RIPA) lysis buffer. The proteins were then separated using Sodium Dodecyl Sulfate-Polyacrylamide Gel Electrophoresis (SDS-PAGE) with a 10% gel. The transfer was executed onto a PVDF membrane (EMD Millipore, Bedford, USA). The membranes were then incubated with the following primary antibodies: anti-SMURF2 at a dilution of 1:800 (Proteintech, Wuhan, China), anti-SIRT1 at 1:1000 (Abcam, Shanghai, China), anti-iNOS and anti-CD206 both at 1:500 (Abmart, Shanghai, China), anti-FOXA2 at 1:1000 (Abcam, Cambridge, UK), and anti-β-Tubulin at 1:10,000 (Abmart, Shanghai, China). Incubation with primary antibodies was performed on a shaker at 4°C overnight. This was followed by a 1 h incubation with the secondary antibodies, either horseradish peroxidase-conjugated anti-mouse or anti-rabbit antibodies (Abmart, Shanghai, China). For semi-quantitative analysis of the protein bands, the Quantity One software (Bio-Rad Laboratories, Milan, Italy) was utilized.

## 2.9 Enzyme-linked immunosorbent assay

Spinal cord tissue was washed with pre-chilled saline, cut into small pieces, and homogenized by adding pre-chilled RIPA protein lysate containing PMSF. Following centrifugation, the supernatant was separated for cytokine testing. HAPI cells were disrupted, and centrifuged, and the supernatant collected for cytokine testing. TNF-α and IL-4 levels were determined using specific ELISA kits (Nanjing Jiancheng Bioengineering, China) according to the manufacturer's instructions. Absorbance was measured at a wavelength of 450 nanometers using a microplate reader. The average values were calculated using a three-hole testing method.

## 2.10 Immunofluorescence

The spinal cords from the L4-L6 segments were sectioned and fixed in 4% paraformaldehyde for a period of 2–4 h. Thereafter, the tissues were cryopreserved overnight at 4°C in 30% sucrose phosphate buffer. Subsequently, the tissues were cut into sections 10 μm thick using a Leica CM 3050s cryostat (Leica Biosystems, USA). To block non-specific binding, the sections were incubated in 10% bovine serum albumin (BSA) for 1 h at room temperature. For immunofluorescence staining, the sections were then incubated

overnight at 4°C with primary antibodies, including anti-iNOS, anti-CD206, anti-SMURF2, anti-SIRT1, and anti-IBA-1 (1:150, Novus, Shanghai, China). Following this, the sections were incubated with secondary antibodies: Dylight 594-affinipure donkey anti-rabbit IgG (1:500, Boster, Wuhan, China) and Alexa 488-conjugated donkey anti-Goat IgG (1:500, Abcam, Shanghai, China) for 1 h at room temperature, followed by staining with DAPI for 5 minutes. For cell samples, the fixed cells were permeabilized following a 4% paraformaldehyde incubation and blockade at room temperature, cells were incubated overnight with primary antibodies anti-iNOS and anti-CD206 (1:150, Shanghai, China) and stained with DAPI after incubation with secondary antibodies for 1 h at room temperature. Finally, images were captured using a universal fluorescence microscope (Nikon, Tokyo, Japan) equipped with an attached digital camera.

## 2.11 Cell counting kit-8 assay

Cells were seeded in 96-well plates at a density of  $5 \times 10^3$  cells/well in 100 μL of complete culture medium and incubated overnight at 37°C under 5% CO<sub>2</sub> to allow adherence. After 24 hours of treatment with miR-mimic, NC mimic, or control, 10 μL of CCK-8 reagent was added to each well, and the plates were further incubated for 2 hours at 37°C. Absorbance was measured at 450 nm using the enzyme-linked immunosorbent assay reader. Wells containing culture medium and CCK-8 reagent without cells served as blanks. All experiments were performed in quintuplicate.

## 2.12 Real-time quantitative reverse transcription PCR

Total RNA was extracted using an RNAiso Plus reagent (Takara, Beijing, China) as per the manufacturer's instructions. For cDNA synthesis, 1 μg of RNA was reverse-transcribed using the PrimeScript<sup>TM</sup> RT reagent Kit with gDNA Eraser (Takara, Beijing, China). Quantitative real-time PCR (RT-qPCR) analysis was carried out using TB GREEN Premix Ex Taq<sup>TM</sup> II (Takara, Beijing, China) on a standard qPCR system. GAPDH and U6 were used as internal reference genes. The data were calculated by the 2-ΔΔCt method, and the experiment was repeated three times independently. The primer sequences used for amplification are provided in [Supplementary Table S1](#).

## 2.13 Dual-luciferase reporter assay

In order to verify SMURF2 targeting by miR-148a-3p, the SMURF2 wild-type 3' untranslated region (3'UTR) containing the miR-148a-3p binding site and the SMURF2 mutant 3'UTR were serially inserted into the pmirGLO vector. Subsequently, HEK293T cells were seeded in 24-well plates at a density of  $2 \times 10^4$  per well and cultured to 60% confluency. Subsequently, the cells were cotransfected with the recombinant plasmid (wild-type/mutant)

and miR-148a-3p mimic or negative control (NC) mimic 24 hours later, along with Renilla luciferase vector as an internal control. Luciferase activity was measured 48 hours after transfection using the Dual-Luciferase Reporter Assay System (Promega, Beijing, China) according to the manufacturer's instructions.

In order to investigate the effect of FOXA2 on miR-148a-3p transcriptional activity, wild-type miR-148a-3p promoter and FOXA2 binding site mutants were inserted into the pGL3-Basic vector. The resulting constructs were then co-transfected into HEK293T cells with pcDNA3.1-FOXA2 overexpressing constructs or empty vectors. Luciferase activity was measured 48 hours after transfection. Firefly luciferase activity was normalized to Renilla luciferase activity to account for transfection efficiency.

## 2.14 Co-immunoprecipitation

The FOXA2 antibody or SMURF2 antibody was coupled with protein A/G agarose beads (Takara Biotechnology, Dalian, China) at 4°C for 1 hour. Following this, the cells were washed with pre-chilled phosphate-buffered saline (PBS). Thereafter, the cells were lysed on ice using Pierce IP lysis buffer (Thermo Fisher Scientific) for 30 minutes. The resulting supernatant was then incubated overnight at 4°C with rotation with antibody-conjugated agarose beads. Thereafter, the precipitated complex was washed with wash buffer and eluted with elution buffer. The eluted samples were subsequently analyzed using Western blot. IgG isotype served as the negative control.

## 2.15 Chromatin immunoprecipitation assay

Subsequent to crosslinking the cells with 1% formaldehyde at room temperature for 10 minutes, the reaction was terminated with 125 mM glycine. Thereafter, the cells were lysed to collect the chromatin. The DNA was fragmented using sonication and then co-cubated overnight at 4°C with FOXA2 antibody or isotype-matched control IgG. The incubation period was overnight at 4°C. Antibody-protein-DNA complexes were isolated by immunoprecipitation using Protein A Sepharose beads. Following a thorough washing procedure, the bound DNA fragments were eluted and subsequently analyzed by RT-qPCR. The primer sequences are listed in the [Supplementary Table S1](#).

## 2.16 Statistical analysis

Prism GraphPad 9.5.0 and IBM SPSS 27 were utilized for the consolidation and statistical analysis of experimental data, presenting results as means ± SEM. To examine the distribution of the data, the Shapiro-Wilk normality test was used. Differences were evaluated using the unpaired t-test between the two groups if data were normally distributed and homogeneous variance. For comparisons involving multiple groups, one-way ANOVA was utilized. Repeated-measures analysis of variance was used to

compare the differences between the two groups at different time points.  $P < 0.05$  indicated statistical significance.

## 3 Results

### 3.1 SCIRI induces neuropathic pain and microglia polarization

To investigate post-SCIRI neuropathic pain, PWT and PWL tests were conducted at designated time points following SCIRI or sham operation. It was observed that following SCIRI, rats exhibited a decline in the mechanical pain threshold and a reduction in PWL in the hot plate test. Both the mechanical pain threshold and thermal pain threshold reached their lowest values on the third day ([Figures 1A, B](#)). These findings indicated that SCIRI triggers neuropathic pain. Prior research has demonstrated that neuropathic pain is inextricably linked to microglial polarization ([41](#)). Therefore, we studied the changes in microglia polarization after SCIRI. Spinal cord tissue was collected three days post-surgery, and Western blot was performed to assess the expression levels of the microglia polarization markers iNOS and CD206. The results suggested that SCIRI significantly increased the expression of iNOS and CD206 ([Figures 1C–E](#)). OGD/R was performed on microglia *in vitro* to simulate SCIRI conditions *in vivo*. Similarly, we observed significant elevations in the expressions of iNOS and CD206 ([Figures 1F–H](#)). ELISA analysis corroborated the elevated levels of TNF- $\alpha$ , a pro-inflammatory factor associated with M1 polarization, and IL-4, an anti-inflammatory factor associated with M2 polarization ([Figures 1I, J](#)). Therefore, it is inferred that SCIRI may affect microglia polarization and thus promote the development of neuropathic pain.

### 3.2 SMURF2 regulates microglia polarization by downregulating SIRT1 after SCIRI

It is known that SIRT1 can alleviate neuropathic pain in many ways, and the regulation of microglia polarization is one of the most critical mechanisms ([42](#)). It has been demonstrated that SMURF2, which functions as an E3 ubiquitin ligase, could bind to SIRT1 and facilitate its ubiquitin-dependent degradation ([35](#)). However, the effect of SMURF2 on microglial polarization is not yet available. The expressions of SIRT1 and SMURF2 in the spinal cord at various time points following SCIRI were measured. SIRT1 expression was progressively reduced post-SCIRI, reaching minimal levels by day three ([Figures 2A, B](#)). SMURF2 increased as early as 8 h after injury, peaked between 1–3 days, and subsequently decreased on the fifth day ([Figures 2A, C](#)). The expression trends of SIRT1 and SMURF2 coincided with neuropathic pain in rats after SCIRI, suggesting a potential relationship between these two molecules and post-SCIRI neuropathic pain in rats.

Frozen sections of the L4–L6 spinal cord were obtained from both the sham-operated rats and the rats 3 days after SCIRI.



Immunofluorescence staining was performed on the sections using IBA-1 (green) to label activated microglia. And then, the sections were co-labeled with either SIRT1 (red) or SMURF2 (red) (Figure 2D). The results demonstrated that the number of IBA-1-positive cells increased in the presence of SCIRI. The ratio of the co-localization area of SIRT1 and IBA-1 to the area of IBA-1 was found to decrease. Conversely, following SCIRI, the ratio of SMURF2 and IBA-1 co-localization area to IBA-1 area in the spinal cord was observed to increase. These outcomes indicated that SCIRI activated spinal microglia and altered the expression of SIRT1 and SMURF2 in microglia. (Figures 2D, E). These findings presented that SCIRI activated spinal microglia and changed the expression of SIRT1 and SMURF2 in microglia.

Figures 2F–H illustrated that OGD/R increased the expression of SMURF2 and decreased the expression of SIRT1. However, the knockdown of SMURF2 (Supplementary Figure S1A) reversed the decrease of SIRT1. To evaluate the impact of SMURF2 on microglia polarization, the expressions of iNOS and CD206 were evaluated by Western blot and immunofluorescence. As shown in Figures 2I and J, the reduction in iNOS expression resulting from SMURF2 knockdown can be partially reversed by SIRT1 knockdown (Supplementary Figure S1B). Conversely, the knockdown of SMURF2 led to an increase in CD206 expression, while the knockdown of SIRT1 partially reversed the effect of SMURF2 on CD206 levels. The simultaneous knockdown of SMURF2 and SIRT1 resulted in a partial recovery of the elevated CD206 (Figures 2I, K). The immunofluorescence experiment provided a more visual representation (Figure 2L), which was consistent with the results of the Western blot. Taken together, the above results revealed that SMURF2 regulated microglial polarization via SIRT1 after SCIRI.

### 3.3 miR-148a-3p reduces ubiquitination of SIRT1 by targeting SMURF2

Building on our findings, the expression of SMURF2 was elevated in microglia following the induction of SCIRI or OGD/R, and its involvement in regulating microglia polarization was established. miRNAs can modulate neuropathic pain resulting from spinal cord injury by regulating target genes as previously reported (43). To determine potential miRNAs that could target SMURF2, TargetScan 8.0 and miRDB databases were employed to predict upstream miRNAs. After taking the intersection of the predicted results and excluding those that could potentially bind to SIRT1, 23 miRNAs were identified (Figure 4A). Seven of the identified miRNAs exhibited TargetScan context++ score percentiles exceeding 90, accompanied by miRDB scores exceeding 80 (Figure 4B). In light of prior research, miR-23b-3p and miR-23a-3p inhibited SIRT1 (44, 45), which was inconsistent with the original hypothesis of this study. Subsequently, RT-qPCR was used to determine the expression of five other miRNAs in the injured spinal cord of rats. Only miR-148a-3p was found to decrease after SCIRI (Figure 4C). Dual-luciferase assays confirmed that miR-148a-3p mimic obviously reduced the

luciferase activity in the group of SMURF2-wt but not in the group of SMURF2-mut (Figure 4D). These findings provided evidence that miR-148a-3p could specifically target and bind to the predicted sites in SMURF2.

To investigate the effects and underlying mechanism of miR-148a-3p on SIRT1, plasmids were constructed for overexpressing SMURF2 (Supplementary Figure S2A), and miR-mimic was used for overexpressing miR-148a-3p (Supplementary Figure S2B). To exclude potential confounding effects of miR-148a-3p mimics on cellular viability, we conducted CCK-8 assays in both HAPI and VSC4.1 cells treated with miR-mimic. The results demonstrated no significant alterations in cell viability compared to control groups (Supplementary Figures S2C, D), validating the safety of miR-mimic under these experimental conditions. As is shown in Figures 4E–G, overexpression of miR-148a-3p exhibited a decrease in SMURF2 and an increase in SIRT1. However, overexpression of SMURF2 reverted the up-regulation of SIRT1. It suggested that miR-148a-3p could elevate SIRT1 expression by inhibiting SMURF2 expression. Consistent with previous studies, immunoprecipitation and Western blot revealed that overexpression of SMURF2 led to an increased ubiquitination of SIRT1. Meanwhile, miR-148a-3p reduced SIRT1 ubiquitination, and SMURF2 effectively reverted the decreased ubiquitination of SIRT1 induced by miR-148a-3p (Figures 4H, I). Collectively, these findings displayed that miR-148a-3p decreased the ubiquitination of SIRT1 by suppressing SMURF2, thereby preventing the degradation of SIRT1.

### 3.4 FOXA2/miR-148a-3p/SMURF2 signaling feed-forward loop regulates microglia polarization

As shown in Figures 5A–C, miR-148a-3p promoted the polarization of M2 microglia, manifesting as an increase in CD206 and a decrease in iNOS, and overexpression of SMURF2 led to the restoration of CD206 and iNOS levels. Immunofluorescence results were consistent with the Western blot findings (Figure 5D), suggesting that miR-148a-3p polarizes microglia towards the M2 phenotype by suppressing SMURF2. Interestingly, SMURF2 knockdown significantly increased miR-148a-3p expression levels (Figure 5E). Therefore, it is speculated that SMURF2 was not only the downstream target gene of miR-148a-3p but also the regulatory factor of miR-148a-3p. As a broad E3 ubiquitin ligase, SMURF2 regulates the ubiquitination and degradation of numerous proteins including transcription factors. Given this, we were prompted to investigate whether SMURF2 might be involved in the regulation of miR-148a-3p transcription factor. Next, we predicted transcription factors of miR-148a-3p from the JASPAR, UCSC, and TFDB databases, combining them with the ubiquitination substrate of SMURF2 from Ubibrowser 2.0 database. Two potential molecules, SP1 and FOXA2, were selected (Figure 5F).

Previous studies have shown that SP1 expression elevated following the onset of SCIRI (46, 47), and that up-regulation of

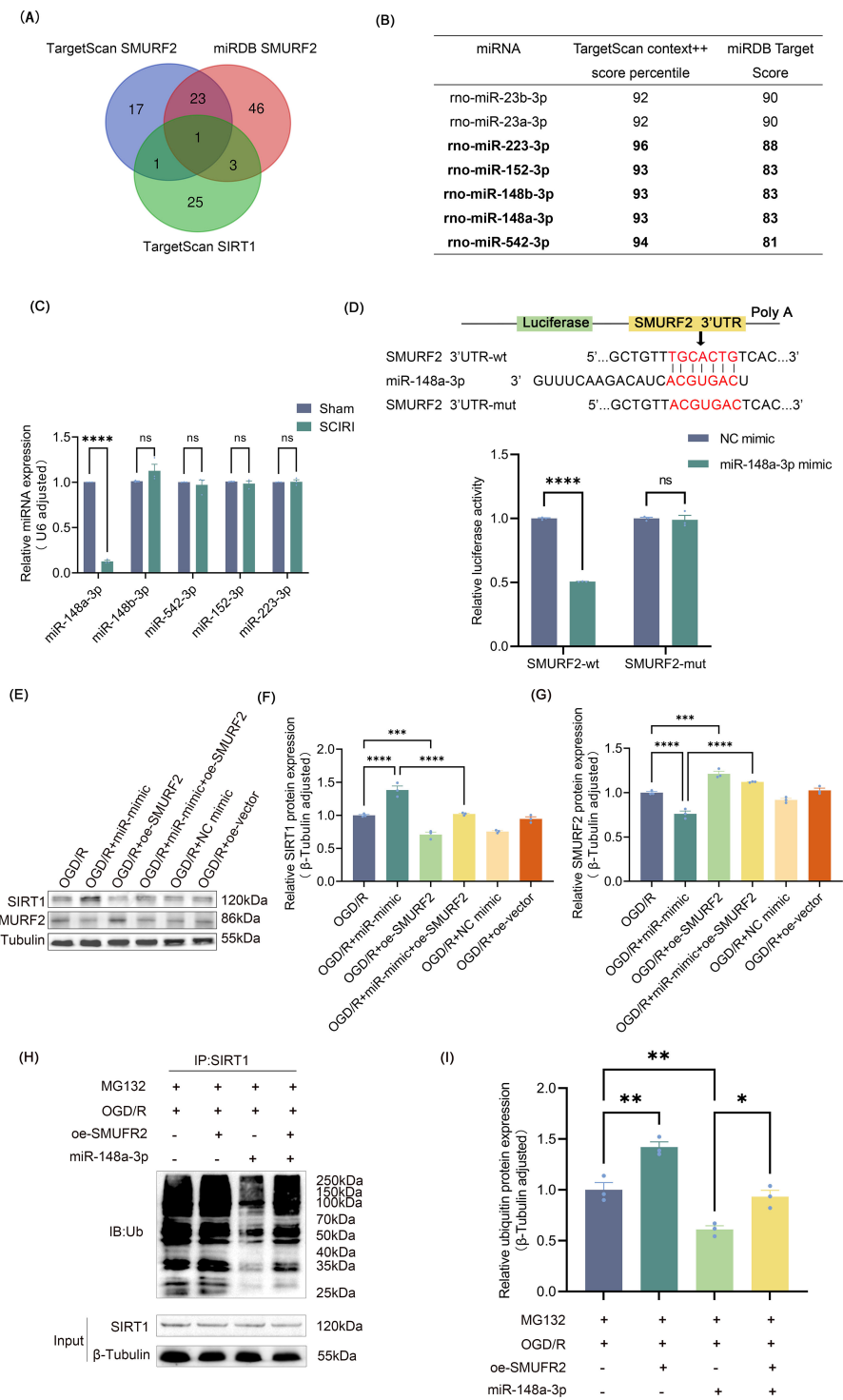


**FIGURE 4** miR-148a-3p reduces ubiquitination of SIRT1 by targeting SMURF2 (A) miRNAs predicted by TargetScan 8.0 and miRDB databases. (B) The selection criteria included miRNAs with TargetScan scores above 90 and miRDB scores above 80. (C) RT-qPCR analysis. (D) Dual-luciferase reporter gene assay. (E) Representative Western blot of SIRT1 and SMURF2. (F, G) Quantitative protein analysis of SIRT1 and SMURF2. (H) Immunoprecipitation followed by Western blot was employed to detect the ubiquitination levels of SIRT1. (I) Quantitative protein analysis of ubiquitin. Unpaired t-test and one-way ANOVA were utilized. Significance levels: \*P<0.05, \*\*P<0.01, \*\*\*P<0.001, \*\*\*\*P<0.0001.

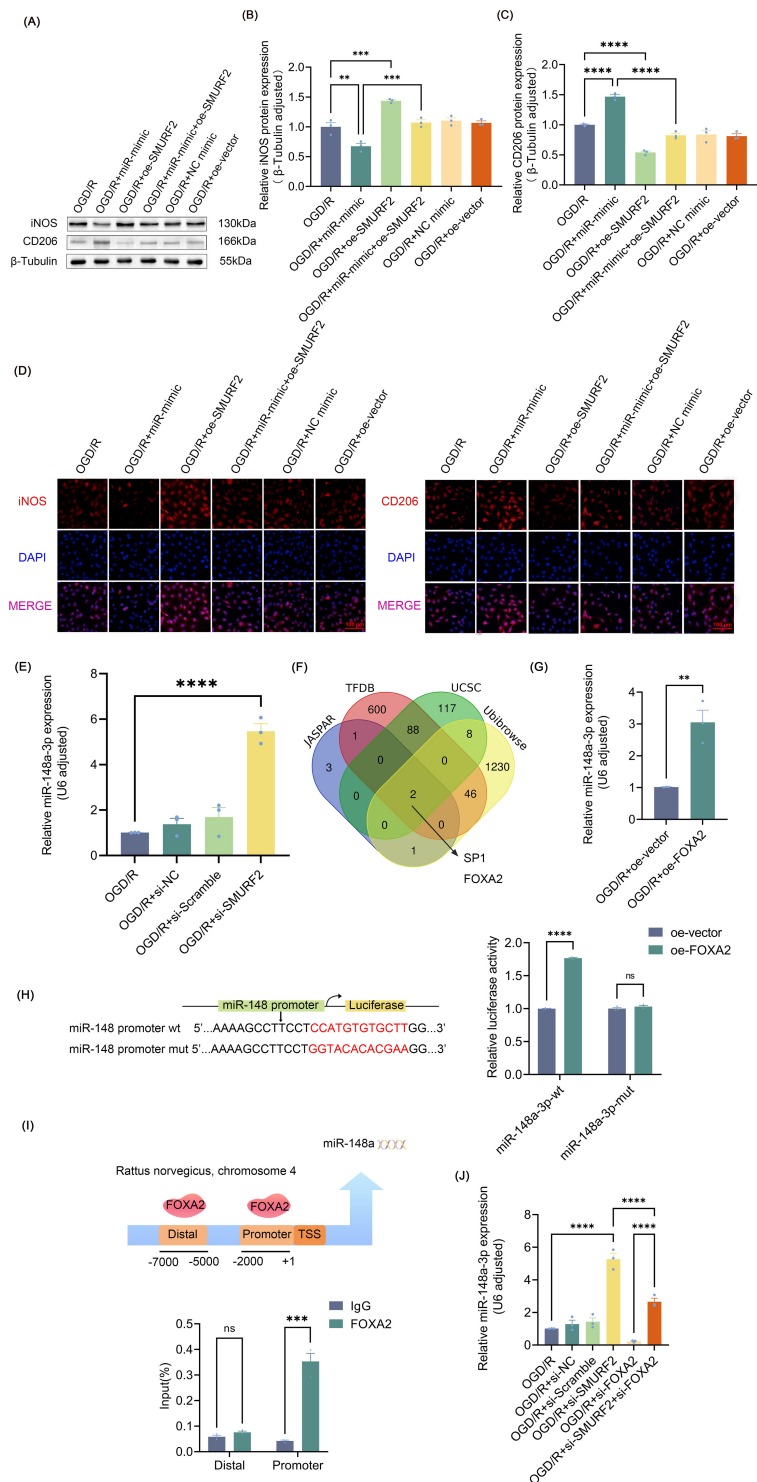


**FIGURE 5**  
FOXA2/miR-148a-3p/SMURF2 signaling feed-forward loop regulates microglia polarization **(A)** Representative Western blot of iNOS and CD206. **(B, C)** Quantitative protein analysis of iNOS and CD206. **(D)** Immunofluorescence revealed iNOS-positive and CD206-positive microglial cells. Scale bar: 100 μm. **(E)** RT-qPCR analysis. **(F)** JASPAR, UCSC, TFDB, and UbiBrowse 2.0 databases were used to predict the potential transcription factors of miR-148a-3p. **(G)** RT-qPCR analysis. **(H)** Dual-luciferase reporter gene assay. **(I)** The binding of FOXA2 to the miR-148a promoters was tested by ChIP assays. **(J)** RT-qPCR analysis. Unpaired t-test and one-way ANOVA were utilized. Significance levels: \*P<0.05, \*\*P<0.01, \*\*\*P<0.001, \*\*\*\*P<0.0001.

SP1 was found to be significantly correlated with the enhancement of prior pain perception (47), which were at odds with the inference of the present study. Therefore, FOXA2 was identified as a suitable subject for further investigation. The results demonstrated a notable elevation in miR-148a-3p expression levels following FOXA2 overexpression (Figure 5G, Supplementary Figure S3A). Subsequently, dual-luciferase reporter gene detection and ChIP assays revealed that FOXA2 was bound to the miR-148a-3p promoter region and regulated its transcriptional activity (Figures 5H, I). Meanwhile, the knockdown of FOXA2 (Supplementary Figure S3B) reversed the effects of SMURF2 on miR-148a-3p (Figure 5J), suggesting that SMURF2 regulated miR-148a-3p through FOXA2. Combined with the previously demonstrated regulation of microglia polarization by inhibition of SMURF2 by miR-148a-3p, it can be concluded that FOXA2/miR-148a-3p/SMURF2 signaling feed-forward loop regulates microglial polarization.

### 3.5 SMURF2 promotes FOXA2 ubiquitination and degradation

To investigate how SMURF2 affects FOXA2, the expression changes of FOXA2 were explored at both mRNA and protein levels, respectively, and the results showed that SMURF2 had no effect on FOXA2 mRNA expression, but significantly inhibited FOXA2 protein expression (Figures 6A, B). The Co-IP assay further confirmed the interaction between SMURF2 and FOXA2 (Figure 6C). Next, we performed ubiquitination validation and found that SMURF2 promoted the ubiquitination of FOXA2, leading to its degradation (Figure 6D). By treating cells with the protein translation inhibitor cycloheximide (CHX), it was shown that the degradation rate of FOXA2 was slowed down after SMURF2 knockdown (Figure 6E). In addition, the ubiquitination degradation of FOXA2 was also restored by the proteasome inhibitor MG132, further confirming that SMURF2 promoted the ubiquitination degradation of FOXA2 (Figure 6F). These results suggested that SMURF2 could reduce FOXA2 protein levels by promoting its ubiquitination and degradation.

### 3.6 Intrathecal injection of miR-148a-3p polarizes spinal microglia to M2 and relieves neuropathic pain after SCIRI

Intrathecal injection of miR-mimic did not improve the mechanical and thermal pain thresholds in the first two days after SCIRI. However, miR-mimic showed beneficial effects on the third day after SCIRI, and this protective effect was further amplified on the following four days (Figures 3B, C). Spinal cord tissues were collected three days after surgery and microglia polarization was measured. Western blot results demonstrated that miR-148a-3p mimic decreased the expression of iNOS and increased the expression of CD206 (Figures 3D–F, Supplementary Figure S4). The results of the ELISA study were in accordance with those of the

Western blot analysis, indicating that the miR-148a-3p mimic resulted in a reduction in TNF- $\alpha$  and an increase in IL-4 (Figure 3G). Additionally, immunofluorescence analysis demonstrated that the miR-148a-3p mimic decreased the co-localization of iNOS with IBA-1 and increased the co-localization of CD206 with IBA-1 (Figures 3H, I). These results indicated that intrathecal injection of miR-148a-3p mitigated neuropathic pain and promoted M2 polarization of microglia following SCIRI.

## 4 Discussion

The presence of neuropathic pain caused by SCIRI has a significant impact on patient outcomes. However, due to the complex mechanism, there is no recognized effective treatment. The present study demonstrated that SCIRI regulated microglial polarization, thereby inducing neuropathic pain. FOXA2/miR-148a-3p/SMURF2 feedback loop was involved in microglial polarization by regulating SIRT1 levels. Intrathecal injection of miR-148a-3p promoted the polarization of spinal microglia to M2 and alleviated neuropathic pain after SCIRI in rats.

It is well-established that microglia polarization is closely associated with neuropathic pain (48, 49). SIRT1 can influence the polarization of microglia through multiple pathways (50–52). As for how to improve the beneficial effects of SIRT1, previous studies focused on enhancing the catalytic activity of SIRT1 but ignored the SIRT1 homeostasis at the protein level (53, 54). SMURF2, a HECT-type E3 ubiquitin ligase, is known to specifically bind to SIRT1, mediating its ubiquitination and degradation in the cytoplasm (35). In this study, SCIRI-induced hyperalgesia was accompanied by increased polarization of microglia. SMURF2 was up-regulated and SIRT1 was down-regulated in spinal microglia after SCIRI. Subsequent experiments showed that SMURF2 promoted the polarization of microglia towards the M1 phenotype by reducing SIRT1 levels.

miR-148a-3p has been proven to bind with numerous target genes, playing a regulatory role in cancer, inflammation, and metabolism (55, 56). For instance, miR-148a-3p can suppress histone deacetylase 5 and enhance cancer cell invasion and migration (55). High-throughput sequencing reveals that elevated expression of miR-148a-3p in human umbilical cord mesenchymal stem cells may foster the polarization of M2 macrophages, thereby potentially mitigating the severity of osteoarthritis (57). To explore the upstream mechanism of SMURF2, we predicted and subsequently confirmed that SMURF2 is a target gene for miR-148a-3p. The results showed that miR-148a-3p inhibited SIRT1 ubiquitination degradation by targeting SMURF2 and promoted microglia polarization toward M2.

It is noteworthy that our findings indicated that SMURF2 could affect miR-148a-3p expression. Therefore, we postulated that SMURF2 functions as an E3 ubiquitin ligase to regulate upstream miR-148a-3p, thereby reversing the regulation of miR-148a-3p. By predicting miRNA transcription factors and SMURF2 ubiquitination substrates, we focused on FOXA2. Subsequent experiments confirmed that FOXA2, as a transcription factor,

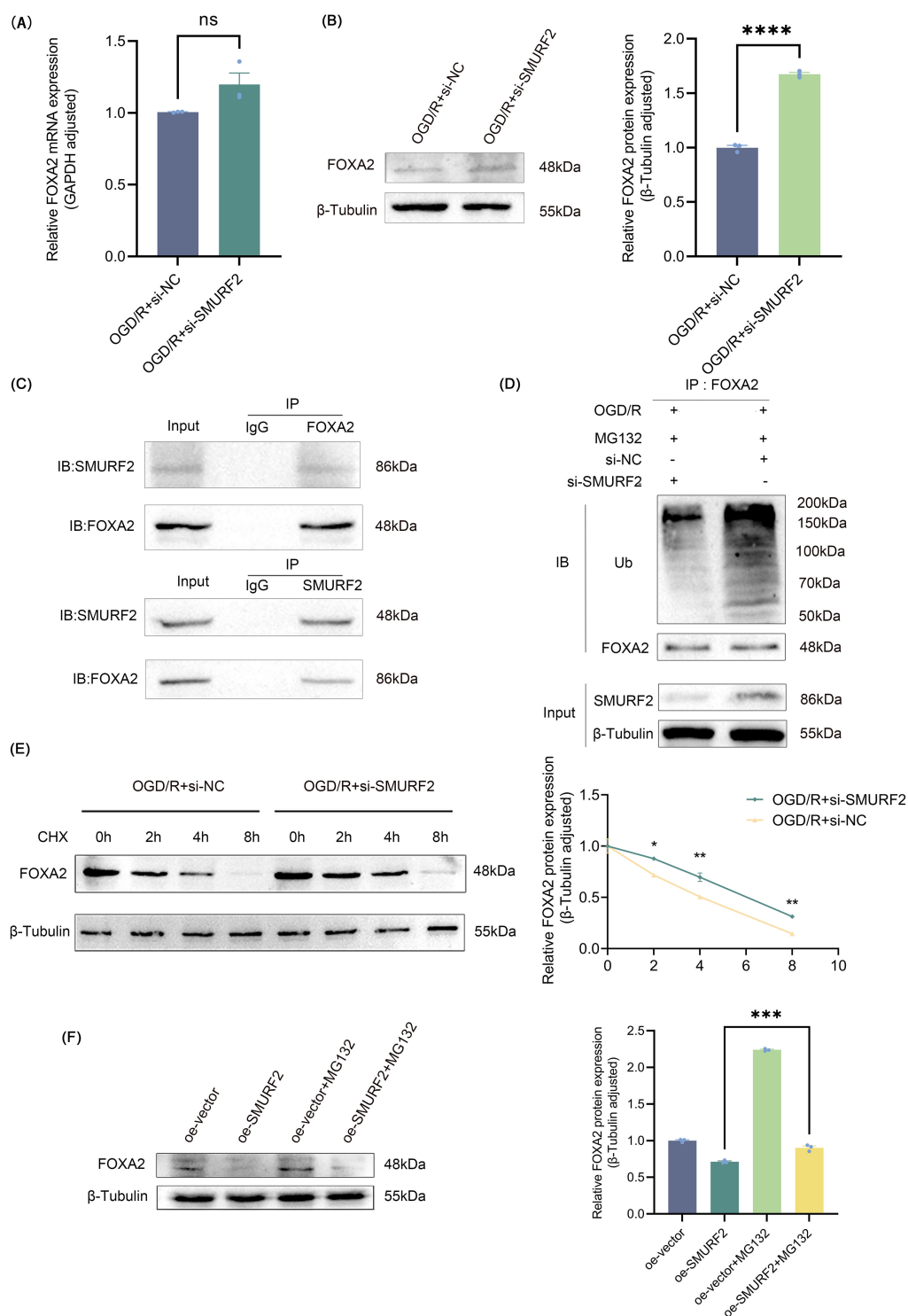


FIGURE 6

SMURF2 promotes FOXA2 ubiquitination and degradation. **(A)** RT-qPCR analysis. **(B)** Representative Western blot of FOXA2 and quantitative protein analysis of FOXA2. **(C)** Co-IP assay suggested protein-protein interactions between SMURF2 and FOXA2. **(D)** Detection of ubiquitination level of FOXA2 by Co-IP. **(E)** Western blot analysis of FOXA2 protein levels treated with CHX. **(F)** Western blot analysis of FOXA2 protein levels treated with MG132. Unpaired t-test and one-way ANOVA were utilized. Significance levels: \* $P < 0.05$ , \*\* $P < 0.01$ , \*\*\* $P < 0.001$ , \*\*\*\* $P < 0.0001$ , ns indicates no significant difference ( $P \geq 0.05$ ).



transcriptionally regulated miR-148a-3p. Additionally, it was found that SMURF2 could bind to FOXA2 and promote FOXA2 ubiquitination and degradation. Further animal experiments demonstrated that intrathecal injection of miR-148a-3p could effectively polarize spinal microglia to the M2 type and alleviate neuropathic pain (Figure 7).

Recent studies have established miRNAs as promising diagnostic and prognostic biomarkers across various diseases (58–60), while extracellular vesicle (EV)-based delivery systems have demonstrated significant therapeutic potential for targeted interventions (61). For example, erythrocyte-derived EVs effectively delivered anti-miR-214 oligonucleotides to suppress pathological bone resorption (62), and CD33-targeted EVs carrying miR-125b antisense oligonucleotides enhanced leukemia stem cell clearance (63). Building on these advancements, future

investigations should explore the dual utility of engineered EVs for both targeted delivery of miR-148a-3p to modulate neuropathic pain through microglial polarization and concurrent development as companion diagnostic biomarkers for neurological disorders. While the study established the FOXA2/miR-148a-3p/SMURF2 axis as a critical regulator of microglial polarization, it is imperative to acknowledge that this regulatory network may be influenced by numerous additional factors. Notably, prior work has shown that miR-148a-3p is involved in the lncRNA-H19/Rock2 axis in regulating oxidative stress in myocardial ischemia-reperfusion injury (64) and targeted PTEN to amplify proinflammatory responses (65). These findings suggest that the FOXA2/miR-148a-3p/SMURF2 axis may be dynamically regulated by multiple factors, and future research should focus on these interactions network between multiple upstream and downstream

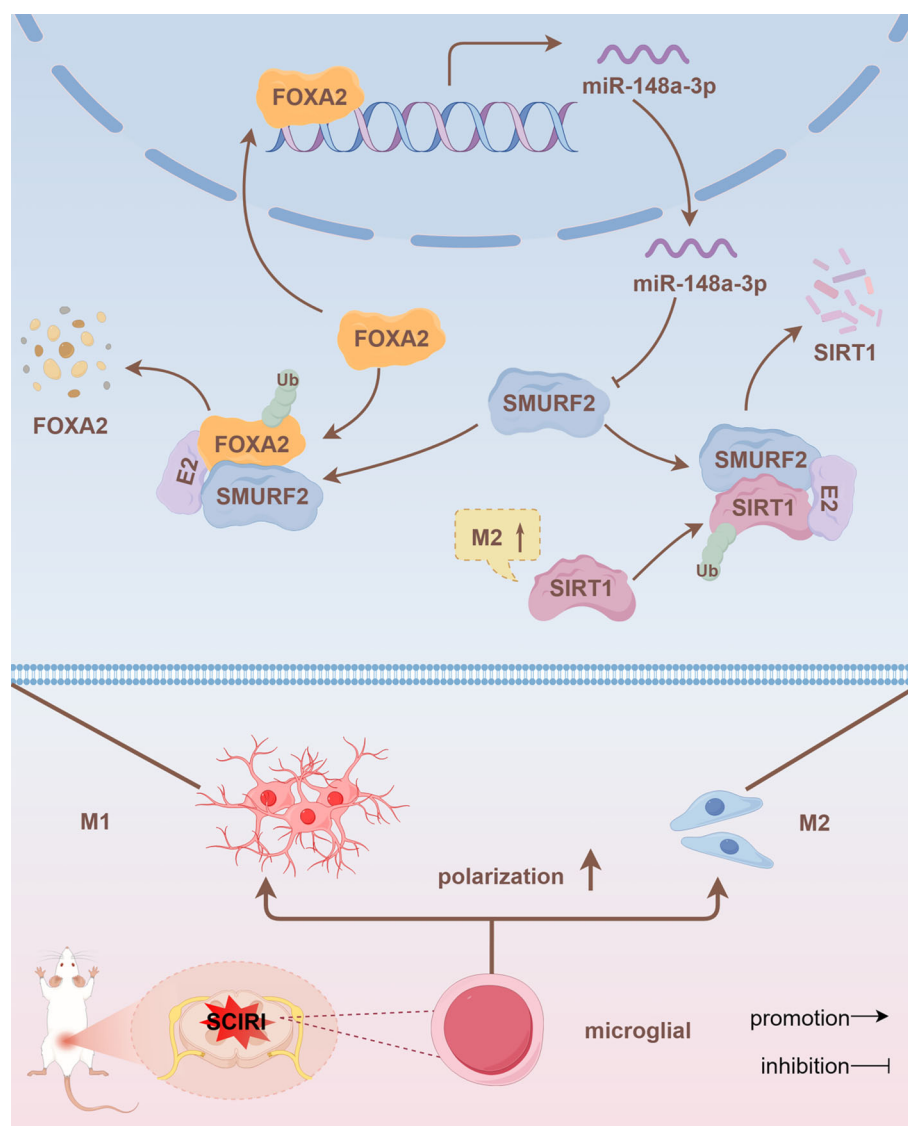


FIGURE 7

FOXA2/miR-148a-3p/SMURF2 feedback loop regulates SIRT1 ubiquitination, affecting microglia polarization and thereby regulating neuropathic pain.

factors of miR-148a-3p to deepen the understanding of the mechanisms underlying neuropathic pain.

## 5 Conclusion

FOXA2/miR-148a-3p/SMURF2 signaling feed-forward loop is involved in SIRT1 ubiquitination and microglia polarization, regulating SCIRI-induced neuropathic pain. Intrathecal administration targeting miR-148a-3p represents a promising therapeutic strategy for clinical intervention in neuropathic pain by reversing the dysregulation of this signaling axis.

## Data availability statement

The original contributions presented in the study are included in the article/Supplementary Material. Further inquiries can be directed to the corresponding author/s.

## Ethics statement

The animal study was approved by Institutional Animal Care and Use Committee of China Medical University. The study was conducted in accordance with the local legislation and institutional requirements.

## Author contributions

XH: Methodology, Validation, Visualization, Writing – original draft, Writing – review & editing, Conceptualization, Data curation, Formal Analysis. LC: Methodology, Writing – original draft, Conceptualization, Formal Analysis. JL: Methodology, Writing – original draft, Data curation, Formal Analysis. QL: Formal Analysis, Supervision, Visualization, Writing – original draft. XL: Formal Analysis, Project administration, Writing – original draft. YL: Conceptualization, Validation, Writing – review & editing. YF: Conceptualization, Visualization, Writing – review & editing. JX: Writing – review & editing, Conceptualization, Visualization. BF: Funding acquisition, Resources, Writing – review & editing.

## References

1. Li K, Yang J, Wang H, Chang X, Liu G, Xue R, et al. Time varying characteristic in somatosensory evoked potentials as a biomarker of spinal cord ischemic-reperfusion injury in rat. *Front Neurosci-Switz.* (2024) 18:1411016. doi: 10.3389/fnins.2024.1411016
2. Sueda T, Takahashi S. Spinal cord injury as a complication of thoracic endovascular aneurysm repair. *Surg Today.* (2018) 48:473–7. doi: 10.1007/s00595-017-1588-5
3. Lu X, Lv C, Zhao Y, Wang Y, Li Y, Ji C, et al. TSG-6 released from adipose stem cells-derived small extracellular vesicle protects against spinal cord ischemia reperfusion injury by inhibiting endoplasmic reticulum stress. *Stem Cell Res Ther.* (2022) 13:291. doi: 10.1186/s13287-022-02963-4
4. Yu Z, Liu J, Sun L, Wang Y, Meng H. Combination of Botulinum Toxin and minocycline Ameliorates Neuropathic Pain Through Antioxidant Stress and Anti-Inflammation via Promoting SIRT1 Pathway. *Front Pharmacol.* (2020) 11:602417. doi: 10.3389/fphar.2020.602417
5. Guida F, De Gregorio D, Palazzo E, Ricciardi F, Boccella S, Belardo C, et al. Behavioral, biochemical and electrophysiological changes in spared nerve injury model of neuropathic pain. *Int J Mol Sci.* (2020) 21:9. doi: 10.3390/ijms21093396
6. Inoue K. Microglia in neuropathic pain. *Adv Neurobiol.* (2024) 37:399–403. doi: 10.1007/978-3-031-55529-9\_22
7. Song ZH, Song XJ, Yang CL, Cao P, Mao Y, Jin Y, et al. Up-regulation of microglial chemokine CXCL12 in anterior cingulate cortex mediates neuropathic pain

## Funding

The author(s) declare that financial support was received for the research and/or publication of this article. This work was supported by the National Natural Science Foundation of China (No. 81971152); Applied basic research Program of Liaoning Province (No. 2023JH2/101300028).

## Acknowledgments

We thank the drawing tools provided by Figdraw 2.0.

## Conflict of interest

The authors declare that the research was conducted in the absence of any commercial or financial relationships that could be construed as a potential conflict of interest.

## Generative AI statement

The author(s) declare that no Generative AI was used in the creation of this manuscript.

## Publisher's note

All claims expressed in this article are solely those of the authors and do not necessarily represent those of their affiliated organizations, or those of the publisher, the editors and the reviewers. Any product that may be evaluated in this article, or claim that may be made by its manufacturer, is not guaranteed or endorsed by the publisher.

## Supplementary material

The Supplementary Material for this article can be found online at: <https://www.frontiersin.org/articles/10.3389/fimmu.2025.1563377/full#supplementary-material>

- in diabetic mice. *Acta Pharmacol Sin.* (2023) 44:1337–49. doi: 10.1038/s41401-022-01046-7
8. Tansley S, Gu N, Guzman AU, Cai W, Wong C, Lister KC, et al. Microglia-mediated degradation of perineuronal nets promotes pain. *Science.* (2022) 377:80–6. doi: 10.1126/science.abl6773
9. Ginhoux F, Greter M, Leboeuf M, Nandi S, See P, Gokhan S, et al. Fate mapping analysis reveals that adult microglia derive from primitive macrophages. *Science.* (2010) 330:841–5. doi: 10.1126/science.1194637
10. Hammond TR, Dufort C, Dissing-Olesen L, Giera S, Young A, Wysoker A, et al. Single-cell RNA sequencing of microglia throughout the mouse lifespan and in the injured brain reveals complex cell-state changes. *Immunity.* (2019) 50:253–71. doi: 10.1016/j.immuni.2018.11.004
11. Wang L, Liu T, Wang X, Tong L, Chen G, Zhou S, et al. Microglia-derived TNF- $\alpha$  contributes to RVLN neuronal mitochondrial dysfunction via blocking the AMPK-Sirt3 pathway in stress-induced hypertension. *J Neuroinflamm.* (2023) 20:137. doi: 10.1186/s12974-023-02818-6
12. Honjoh K, Nakajima H, Hirai T, Watanabe S, Matsumine A. Relationship of inflammatory cytokines from M1-type microglia/macrophages at the injured site and lumbar enlargement with neuropathic pain after spinal cord injury in the CCL21 knockout (plt) mouse. *Front Cell Neurosci.* (2019) 13:525. doi: 10.3389/fncel.2019.00525
13. Timofeeva AV, Akhmetzyanova ER, Rizvanov AA, Mukhamedshina YO. Interaction of microglia with the microenvironment in spinal cord injury. *Neuroscience.* (2025) 565:594–603. doi: 10.1016/j.neuroscience.2024.11.074
14. Orihuela R, McPherson CA, Harry GJ. Microglial M1/M2 polarization and metabolic states. *Brit J Pharmacol.* (2016) 173:649–65. doi: 10.1111/bph.v173.4
15. Hsu CH, Pan YJ, Zheng YT, Lo RY, Yang FY. Ultrasound reduces inflammation by modulating M1/M2 polarization of microglia through STAT1/STAT6/PPARGamma signaling pathways. *CNS Neurosci Ther.* (2023) 29:4113–23. doi: 10.1111/cns.14333
16. Han S, Yuan X, Zhao F, Manyande A, Gao F, Wang J, et al. Activation of LXRs alleviates neuropathic pain-induced cognitive dysfunction by modulation of microglia polarization and synaptic plasticity via PI3K/AKT pathway. *Inflammation Res.* (2024) 73:157–74. doi: 10.1007/s00011-023-01826-9
17. Li H, Wang P, Tang L, Sun J, Zhang Y, Luo W, et al. Distinct polarization dynamics of microglia and infiltrating macrophages: A novel mechanism of spinal cord ischemia/reperfusion injury. *J Inflammation Res.* (2021) 14:5227–39. doi: 10.2147/JIR.S335382
18. Akhmetzyanova ER, Zhuravleva MN, Timofeeva AV, Tazetdinova IG, Garanina EE, Rizvanov AA, et al. Severity- and time-dependent activation of microglia in spinal cord injury. *Int J Mol Sci.* (2023) 24:8294. doi: 10.3390/ijms24098294
19. Zhao Y, Li T, Zhang L, Yang J, Zhao F, Wang Y, et al. TRAF6 promotes spinal microglial M1 polarization to aggravate neuropathic pain by activating the c-JUN/NF- $\kappa$ B signaling pathway. *Cell Biol Toxicol.* (2024) 40:54. doi: 10.1007/s10565-024-09900-6
20. Gao L, Zhang AP, Fu L, Li QW, Qin XM, Zhao J. Huangqin decoction attenuates spared nerve injury (SNI)-induced neuropathic pain by modulating microglial M1/M2 polarization partially mediated by intestinal nicotinamide metabolism. *Phytomedicine.* (2024) 129:155594. doi: 10.1016/j.phymed.2024.155594
21. Wang X, Jiang Y, Li J, Wang Y, Tian Y, Guo Q, et al. DUSP1 Promotes Microglial Polarization toward M2 Phenotype in the Medial Prefrontal Cortex of Neuropathic Pain Rats via Inhibition of MAPK Pathway. *ACS Chem Neurosci.* (2021) 12:966–78. doi: 10.1021/acscchemneuro.0c00567
22. Gui X, Wang H, Wu L, Tian S, Wang X, Zheng H, et al. Botulinum toxin type A promotes microglial M2 polarization and suppresses chronic constriction injury-induced neuropathic pain through the P2X7 receptor. *Cell Biosci.* (2020) 10:45. doi: 10.1186/s13578-020-00405-3
23. Lan X, Han X, Li Q, Li Q, Gao Y, Cheng T, et al. Pinocembrin protects hemorrhagic brain primarily by inhibiting toll-like receptor 4 and reducing M1 phenotype microglia. *Brain Behav Immun.* (2017) 61:326–39. doi: 10.1016/j.bbi.2016.12.012
24. Yao K, Mou Q, Lou X, Ye M, Zhao B, Hu Y, et al. Microglial SIRT1 activation attenuates synapse loss in retinal inner plexiform layer via mTORC1 inhibition. *J Neuroinflamm.* (2023) 20:202. doi: 10.1186/s12974-023-02886-8
25. Wen Q, Wang Y, Pan Q, Tian R, Zhang D, Qin G, et al. MicroRNA-155-5p promotes neuroinflammation and central sensitization via inhibiting SIRT1 in a nitroglycerin-induced chronic migraine mouse model. *J Neuroinflamm.* (2021) 18:287. doi: 10.1186/s12974-021-02342-5
26. Zhang Y, Anoopkumar-Dukie S, Mallik SB, Davey AK. SIRT1 and SIRT2 modulators reduce LPS-induced inflammation in HAPI microglial cells and protect SH-SY5Y neuronal cells *in vitro*. *J Neural Transm.* (2021) 128:631–44. doi: 10.1007/s00702-021-02331-1
27. Yin Q, Lu FF, Zhao Y, Cheng MY, Fan Q, Cui J, et al. Resveratrol facilitates pain attenuation in a rat model of neuropathic pain through the activation of spinal Sirt1. *Region Anesth Pain M.* (2013) 38:93–9. doi: 10.1097/AAP.0b013e3182795b23
28. Chen K, Fan J, Luo ZF, Yang Y, Xin WJ, Liu CC. Reduction of SIRT1 epigenetically upregulates NALP1 expression and contributes to neuropathic pain induced by chemotherapeutic drug bortezomib. *J Neuroinflamm.* (2018) 15:292. doi: 10.1186/s12974-018-1327-x
29. He S, Jiang X, Yang J, Wu Y, Shi J, Wu X, et al. Nicotinamide mononucleotide alleviates endotoxin-induced acute lung injury by modulating macrophage polarization via the SIRT1/NF- $\kappa$ B pathway. *Pharm Biol.* (2024) 62:22–32. doi: 10.1080/13880209.2023.2292256
30. Su H, Fan S, Zhang L, Qi H. TMAO aggregates neurological damage following ischemic stroke by promoting reactive astrogliosis and glial scar formation via the smurf2/ALK5 axis. *Front Cell Neurosci.* (2021) 15:569424. doi: 10.3389/fncel.2021.569424
31. Liu Y, Li YP, Xiao LM, Chen LK, Zheng SY, Zeng EM, et al. Extracellular Vesicles Derived from Bone Mesenchymal Stem Cells Carrying circ\_0000075 Relieves Cerebral Ischemic Injury by Competitively Inhibiting miR-218-5p and Up-regulating E3 Ubiquitin Ligase SMURF2. *Mol Neurobiol.* (2023) 60:2801–18. doi: 10.1007/s12035-022-03192-9
32. Stuelten CH, Melis N, Subramanian B, Tang Y, Kimicata M, Fisher JP, et al. Smurf2 regulates inflammation and collagen processing in cutaneous wound healing through transforming growth factor- $\beta$ /smad3 signaling. *Am J Pathol.* (2022) 192:1699–711. doi: 10.1016/j.ajpath.2022.08.002
33. Zheng W, Hou G, Li Y. Circ\_0116061 regulated the proliferation, apoptosis, and inflammation of osteoarthritis chondrocytes through regulating the miR-200b-3p/SMURF2 axis. *J Orthop Surg Res.* (2021) 16:253. doi: 10.1186/s13018-021-02391-9
34. Popova A, Kzhyshkowska J, Nurgazieva D, Goerdts S, Gratchev A. Smurf2 regulates IL17RB by proteasomal degradation of its novel binding partner DAZAP2. *Immunobiology.* (2012) 217:321–8. doi: 10.1016/j.imbio.2011.10.004
35. Yu L, Dong L, Li H, Liu Z, Luo Z, Duan G, et al. Ubiquitination-mediated degradation of SIRT1 by SMURF2 suppresses CRC cell proliferation and tumorigenesis. *Oncogene.* (2020) 39:4450–64. doi: 10.1038/s41388-020-1298-0
36. Hao LY, Zhang M, Tao Y, Xu H, Liu Q, Yang K, et al. miRNA-22 upregulates mtfl in dorsal horn neurons and is essential for inflammatory pain. *Oxid Med Cell Longev.* (2022) 2022:8622388. doi: 10.1155/2022/8622388
37. Qi R, Cao J, Sun Y, Li Y, Huang Z, Jiang D, et al. Histone methylation-mediated microRNA-32-5p down-regulation in sensory neurons regulates pain behaviors via targeting Cav3.2 channels. *P Natl Acad Sci USA.* (2022) 119:e2117209119. doi: 10.1073/pnas.2117209119
38. Yang S, Jiang Y, Ren X, Feng D, Zhang L, He D, et al. FOXA1-induced circOSBP10 potentiates cervical cancer cell proliferation and migration through miR-1179/UBE2Q1 axis. *Cancer Cell Int.* (2020) 20:389. doi: 10.1186/s12935-020-01360-2
39. Peng Q, Zhang L, Li J, Wang W, Cai J, Ban Y, et al. FOXA1 Suppresses the Growth, Migration, and Invasion of Nasopharyngeal Carcinoma Cells through Repressing miR-100-5p and miR-125b-5p. *J Cancer.* (2020) 11:2485–95. doi: 10.7150/jca.40709
40. Wu C, Xu H, Li J, Hu X, Wang X, Huang Y, et al. Baicalein attenuates pyroptosis and endoplasmic reticulum stress following spinal cord ischemia-reperfusion injury via autophagy enhancement. *Front Pharmacol.* (2020) 11:1076. doi: 10.3389/fphar.2020.01076
41. Li X, Shi H, Zhang D, Jing B, Chen Z, Zheng Y, et al. Paeonol alleviates neuropathic pain by modulating microglial M1 and M2 polarization via the RhoA/p38MAPK signaling pathway. *CNS Neurosci Ther.* (2023) 29:2666–79. doi: 10.1111/cns.14211
42. An M, Qiu Y, Wang C, Ma P, Ding Y. Rac2 enhances activation of microglia and astrocytes, inflammatory response, and apoptosis via activating JNK signaling pathway and suppressing SIRT1 expression in chronic constriction injury-induced neuropathic pain. *J Neuropath Exp Neur.* (2023) 82:419–26. doi: 10.1093/jnen/nlad006
43. Sahebdel F, Zia A, Quinta HR, Morse LR, Olson JK, Battaglini RA. Transcriptomic Profiling of Primary Microglia: Effects of miR-19a-3p and miR-19b-3p on Microglia Activation. *Int J Mol Sci.* (2024) 25:10601. doi: 10.3390/ijms251910601
44. Zhao S, Li T, Li J, Lu Q, Han C, Wang N, et al. miR-23b-3p induces the cellular metabolic memory of high glucose in diabetic retinopathy through a SIRT1-dependent signalling pathway. *Diabetologia.* (2016) 59:644–54. doi: 10.1007/s00125-015-3832-0
45. Sruthi TV, Edatt L, Raji GR, Kunhiraman H, Shankar SS, Shankar V, et al. Horizontal transfer of miR-23a from hypoxic tumor cell colonies can induce angiogenesis. *J Cell Physiol.* (2018) 233:3498–514. doi: 10.1002/jcp.v233.4
46. Liu S, Chen F, Han J, Wang L, Dong Y. Ferostatin-1 improves neurological impairment induced by ischemia/reperfusion injury in the spinal cord through ERK1/2/SP1/GPX4. *Exp Neurol.* (2024) 373:114659. doi: 10.1016/j.expneurol.2023.114659
47. Xie Y, Li Z, Xu H, Ma J, Li T, Shi C, et al. Downregulation of sp1 inhibits the expression of HDAC1/SOX10 to alleviate neuropathic pain-like behaviors after spinal nerve ligation in mice. *ACS Chem Neurosci.* (2022) 13:1446–55. doi: 10.1021/acscchemneuro.2c00091
48. Hu X, Du L, Liu S, Lan Z, Zang K, Feng J, et al. A TRPV4-dependent neuroimmune axis in the spinal cord promotes neuropathic pain. *J Clin Invest.* (2023) 133:e161507. doi: 10.1172/JCI161507
49. Silveira PA, Hoon LS, Roh J, Luckemeyer DD, Cohen CF, Pertin M, et al. Microglial STING activation alleviates nerve injury-induced neuropathic pain in male but not female mice. *Brain Behav Immun.* (2024) 117:51–65. doi: 10.1016/j.bbi.2024.01.003
50. Xia DY, Yuan JL, Jiang XC, Qi M, Lai NS, Wu LY, et al. SIRT1 promotes M2 microglia polarization via reducing ROS-mediated NLRP3 inflammasome signaling

after subarachnoid hemorrhage. *Front Immunol.* (2021) 12:770744. doi: 10.3389/fimmu.2021.770744

51. Li J, Yu M, Zong R, Fan C, Ren F, Wu W, et al. Deacetylation of Notch1 by SIRT1 contributes to HBsAg- and HBeAg-mediated M2 macrophage polarization. *Am J Physiol-Gastr L.* (2022) 322:G459–71. doi: 10.1152/ajpgi.00338.2021

52. Wang J, Ma S, Yu J, Zuo D, He X, Peng H, et al. MiR-9-5p promotes M1 cell polarization in osteoarthritis progression by regulating NF-kappaB and AMPK signaling pathways by targeting SIRT1. *Int Immunopharmacol.* (2021) 101:108207. doi: 10.1016/j.intimp.2021.108207

53. Li C, Xue P, Duan G, Song A, Zhai R, Ma J, et al. ED-71 promotes osseointegration of titanium implants in a rat model of GIOP by alleviating the effects of dexamethasone on bone remodeling in a SIRT1-dependent manner. *J Oral Biosci.* (2024) 67:100571. doi: 10.1016/j.job.2024.10.003

54. Liang T, Liu R, Liu J, Hong J, Gong F, Yang X. miRNA506 activates sphk1 binding with sirt1 to inhibit brain injury after intracerebral hemorrhage via PI3K/AKT signaling pathway. *Mol Neurobiol.* (2024) 62:4093–114. doi: 10.1007/s12035-024-04534-5

55. Chen FS, Tong XY, Fang B, Wang D, Li XQ, Zhang ZL. The roles of microRNAs in spinal cord ischemia-reperfusion injury. *Neural Regener Res.* (2022) 17:2593–9. doi: 10.4103/1673-5374.339471

56. Su H, Fan G, Huang J, Qiu X. YBX1 regulated by Runx3-miR-148a-3p axis facilitates non-small-cell lung cancer progression. *Cell Signal.* (2021) 85:110049. doi: 10.1016/j.cellsig.2021.110049

57. Zhang X, Chen F, Huang P, Wang X, Zhou K, Zhou C, et al. Exosome-depleted MiR-148a-3p derived from Hepatic Stellate Cells Promotes Tumor Progression via ITGA5/PI3K/Akt Axis in Hepatocellular Carcinoma. *Int J Biol Sci.* (2022) 18:2249–60. doi: 10.7150/ijbs.66184

58. Khella H, Daniel N, Youssef L, Scorilas A, Nofech-Mozes R, Mirham L, et al. miR-10b is a prognostic marker in clear cell renal cell carcinoma. *J Clin Pathol.* (2017) 70:854–9. doi: 10.1136/jclinpath-2017-204341

59. Roderburg C, Benz F, Vargas CD, Koch A, Janssen J, Vucur M, et al. Elevated miR-122 serum levels are an independent marker of liver injury in inflammatory diseases. *Liver Int.* (2015) 35:1172–84. doi: 10.1111/liv.2015.35.issue-4

60. Perez-Hernandez J, Martinez-Arroyo O, Ortega A, Galera M, Solis-Salguero MA, Chaves FJ, et al. Urinary exosomal miR-146a as a marker of albuminuria, activity changes and disease flares in lupus nephritis. *J Nephrol.* (2021) 34:1157–67. doi: 10.1007/s40620-020-00832-y

61. Chiangjong W, Netsirisawan P, Hongeng S, Chutipongtanate S. Red blood cell extracellular vesicle-based drug delivery: challenges and opportunities. *Front Med-Lausanne.* (2021) 8:761362. doi: 10.3389/fmed.2021.761362

62. Xu L, Xu X, Liang Y, Wen C, Ouyang K, Huang J, et al. Osteoclast-targeted delivery of anti-miRNA oligonucleotides by red blood cell extracellular vesicles. *J Control Release.* (2023) 358:259–72. doi: 10.1016/j.jconrel.2023.04.043

63. Chen H, Jayasinghe MK, Yeo E, Wu Z, Pirisinu M, Usman WM, et al. CD33-targeting extracellular vesicles deliver antisense oligonucleotides against FLT3-ITD and miR-125b for specific treatment of acute myeloid leukaemia. *Cell Proliferat.* (2022) 55: e13255. doi: 10.1111/cpr.13255

64. Zeng J, Zhu L, Liu J, Zhu T, Xie Z, Sun X, et al. Metformin Protects against Oxidative Stress Injury Induced by Ischemia/Reperfusion via Regulation of the lncRNA-H19/miR-148a-3p/Rock2 Axis. *Oxid Med Cell Longev.* (2019) 2019:8768327. doi: 10.1155/2019/8768327

65. Huang F, Zhao JL, Wang L, Gao CC, Liang SQ, An DJ, et al. miR-148a-3p mediates notch signaling to promote the differentiation and M1 activation of macrophages. *Front Immunol.* (2017) 8:1327. doi: 10.3389/fimmu.2017.01327